BMC Genomics

RESEARCH

Open Access

Inference of causal interaction networks of gut microbiota using transfer entropy

Chanho Park[1], Junil Kim[1,2*] and Julian Lee[1,2*]

Abstract

Background Understanding the complex dynamics of gut microbiota interactions is essential for unraveling their influence on human health. However, inferring causality from microbiome time-series data is challenging due to noise, sparsity, and high dimensionality. Constructing causal interaction networks can provide valuable insights into the regulatory mechanisms of the gut microbiome.

Results In this study, we employed transfer entropy analysis to construct a causal interaction network among gut microbiota genera from time-series abundance data. Based on longitudinal microbiome data from two subjects, we found that the constructed gut microbiota regulatory networks exhibited a power-law degree distribution, intermediate modularity, and enrichment of feedback loops. Interestingly, the networks of the two subjects displayed differential enrichment of feedback loops, which may be associated with the differences in their recovery dynamics.

Conclusions The transfer entropy-based network construction approach offers valuable insights into the gut microbiota ecosystem and enables the identification of key microbial hubs that play pivotal roles in shaping microbial balance. This method provides a deeper understanding of microbial regulatory interactions and their potential implications for host health.

Keywords Transfer entropy, Microbiota, Causal interaction network, Microbiome, Feedback loops

Background

The human microbiota, particularly the gut microbiota, plays a crucial role in maintaining our health. This vast and dynamic assembly of microorganisms inhabits various parts of our body, with the gut microbiota being one of the most influential due to its extensive interactions with human physiology. Many studies have shed light on the profound impact the gut microbiota on human health [1–10]. They assist in the digestion and fermentation of the food, enabling the extraction and synthesis of vital nutrients and energy from the food we consume [5, 6]. Beyond their role in nutrition, these microbial communities serve to protect against pathogens [7, 8], regulate immune function, and strengthen the bio-chemical barriers of the gut and intestine [8].

Various bacterial species forming the microbiota interact with each other for their survival. In particular, the network of causal relationships among microbiota is important as it provides insights into the complex and dynamic ecosystem of microorganisms that are critically important in the function of any biological community. These networks can help us understand how commensal

*Correspondence:
Junil Kim
junilkim@ssu.ac.kr
Julian Lee
jul@ssu.ac.kr
[1]Department of Bioinformatics and Life Science, Soongsil University, 369 Sangdo-Ro, Dongjak-Gu, Seoul 06987, Republic of Korea
[2]School of Systems Biomedical Science, Soongsil University, 369 Sangdo-Ro, Dongjak-Gu, Seoul 06987, Republic of Korea

and pathogenic microbiota modulate host signaling and have broad cross-species consequences.

Early studies on microbiota interactions relied on analyzing correlations between them, which produce only undirected interaction networks [11–17]. More detailed information on the nature of interactions can only be obtained by analyzing the time series of bacterial abundances, where directed graphs are obtained [18–21]. While significant progress has been made, the rigorous inference of causal relationships between bacterial species using information theory remains an underexplored area. In this study, we address this gap by constructing a causal interaction network employing transfer entropy (TE) [22], an information-theoretic measure for determining causality between variables.

TE has been used for inferring causal relationships within dynamic systems, including the functional connectivity of neurons [23–25] and transcriptional regulation [26–28], by measuring the information transferred from one agent in the interacting network to another. It has also been applied beyond biology, such as in social systems [22], climate science, and finance—e.g., to reveal directional information flow among global stock indices [26–30]. TENET (Transfer Entropy-based causal gene NETwork) algorithm [26] is designed to construct gene regulatory networks (GRNs) from single-cell RNA sequencing data, demonstrating superior performance in identifying key regulatory transcription factors. Employing TENET, we built the causal interaction network of gut microbiota, by analyzing one-year time series of microbiota data from two individuals [31]. Although TENET was originally developed for scRNA-seq data, it can be applied to microbiome time-series. The core steps of the original TENET pipeline—including transfer entropy computation and non-parametric entropy estimation using kernel density estimation—were preserved as originally implemented. Compared to single-cell gene expression data, microbiome profiles are typically less sparse but compositional in nature. While TENET's estimator offers some robustness, the indirect effect trimming step was used to remove potentially indirect or confounded edges.

The resulting microbiota causal network revealed: (1) a power-law degree distribution with a few super-hub nodes; (2) intermediate modular structure characterized by phylum; and (3) an enrichment of feedback loops. Key bacterial genera, such as *Acrobacter* and *Clostridium*, were pinpointed as central hubs or connectors in these networks, with associations to the hosts' health outcomes or environmental interactions. These findings suggest that TE is a valuable tool for identifying critical regulatory genera within gut microbiota, which could be potential candidates of therapeutic targets.

Methods

Processing of time-series data

One year time-series of gut microbiota for two people have been obtained in David et al. [31]. David et al. generated a sequencing data of V4 region of the 16 S ribosomal RNA gene subunit on DNA obtained from stool samples collected daily from two subjects, subject A for 341 days and subject B for 192 days. The raw data resulting from this work are available in the European Nucleotide Archive (ENA) (https://www.ebi.ac.uk/ena/browser/view/PRJEB6518) maintained by the European Bioinformatics Institute (EBI). Post-processed time-series data are also available at MGnify database (https://www.ebi.ac.uk/metagenomics/studies/MGYS00001278#analysis), at the level of 32 phyla and 879 operational taxonomy units (OTUs). Specifically, we used the MGnify-processed data generated using pipeline version 2.0, which we downloaded in March 2023. We used the time-series data for the OTUs and grouped them according to genera, resulting in the time-series abundances of 667 genera (Supplementary Table S1 and S2). While species-level resolution can provide more specific biological insights, we chose to aggregate OTUs at the genus level for two main reasons. First, genus-level aggregation reduces noise and enhances robustness in detecting temporal patterns and causal relationships in sparse microbiome time-series data [32]. Second, species-level annotations for many OTUs in the MGnify output vary in resolution, making genus-level aggregation a pragmatic choice to ensure consistency and reliability in downstream analysis. Additionally, phylum names were standardized according to recent taxonomic conventions [33].

Construction of gut microbiota regulatory network

TENET algorithm [26] computes transfer entropy for a given pair of components in an interaction network, when time-series for these components are given. The transfer entropy is defined as [22]

$$TE_{X\to Y} \equiv H\left(Y_t|\ Y_{t-1:-L}\right) - H\left(Y_t|\ Y_{t-1:t-L},\ X_{t-1:t-L}\right) \quad (1)$$

where $X_{t-1:t-L}$ and $Y_{t-1:t-L}$ denote the time series for the time-points *t-L*, *t-L + 1*, ... *t-1*, and *H(X)* is the Shannon's entropy:

$$H\left(X\right) \equiv -\sum {}_x p\left(x\right)\log p\left(x\right) \quad (2)$$

with $p\left(x\right)$ being the probability that X takes the value x. The transfer entropy $TE_{X\to Y}$ measures the uncertainty on Y removed by gaining the information on the history of X, and estimate the information flow from X to Y. For estimating conditional entropy, TENET utilized a kernel density estimator, a non-parametric approach to estimate the probability density function of a random variable

[26]. For simplicity, we will consider only the effect of the immediate past of the current time-point and use $L = 1$. We chose $L = 1$ since TENET results was almost similar when $L > 1$ is applied in the original TENET study on single cell RNAseq [26].

TENET [26] was downloaded from github.com/neocaleb/TENET and applied to the time-series microbiota profiles at the genus level for each subject individually. We then represented the microbiota regulatory network as a directed binary graph, where a node represents a genus, and there is a directed edge from a node A to a node B if $TE_{A\rightarrow B}$ is significantly large. To assess the significance of a TE value, we computed a z-score based on the assumption of normally distributed TE values. Edges were retained in the network if their z-scores exceeded a threshold corresponding to a nominal FDR-level cutoff (θ). While this procedure is inspired by the Benjamini-Hochberg approach [34], we note that, according to the original design of the TENET algorithm [26], the p-values are not derived from a null distribution. Instead, z-scores are computed using the empirical distribution of TE values observed across all variable pairs. Thus, θ is used as a tunable stringency parameter rather than as a formal false discovery control. Even if $TE_{A\rightarrow B}$ is significantly large, we did not draw a directed edge from A to B if this is due to an indirect effect, where there is a node C such that A affects C and C affects B, but there is no direct causal effect of A on B. We assume such an indirect influence of A on B when we found C such that $TE_{A\rightarrow B}$ is less than the minimum value of $TE_{A\rightarrow c}$ and $TE_{c\rightarrow B}$. In this case, we did not draw a directed edge from A to B in the final graph. We repeated this trimming process until no further eliminations are necessary.

To test the robustness of the properties of the directed binary network with respect to the FDR threshold θ, we used both $\theta = 0.01$ and $\theta = 0.05$. The constructed networks were visualized using Cytoscape 3.9.1 with "Edge-weighted Force directed" and "Group Attributes" layouts [35].

Correlation-based association network

We constructed an undirected association network by calculating pairwise Spearman rank correlations between genus-level abundance for each subject. The signed correlation coefficient was used as the edge weight, and edges were retained if the two-sided Spearman test P-value was less than 0.05. Self-loops were excluded.

SPIEC-EASI network

We inferred a sparse association network using SPIEC-EASI (Sparse InversE Covariance estimation for Ecological Association and Statistical Inference) [36]. For each subject, genus-level abundance tables were analyzed using the neighborhood-selection formulation to estimate a sparse precision matrix. Model selection used stability selection, and the final undirected graph was defined by the non-zero entries of the refitted precision matrix.

Degree distribution

Many biological networks follow power-law degree distribution [37]. We constructed the degree distribution of each network and fitted the distribution to the power-law equation:

$$p_k = Ck^{-\gamma} \tag{3}$$

where p_k is the distribution or probability of degree k, C is a normalization constant ensuring that the sum of all probabilities p_k over all k equal 1, and γ is the degree exponent.

Leiden clustering

We used Leiden algorithm for community detection of network [38]. Although Leiden clustering algorithm is mainly designed for undirected graphs, we chose Leiden algorithm instead of algorithms for directed graphs, such as directed Louvain algorithm, since Leiden algorithm is more improved algorithm in detecting well-connected communities [38]. We also performed directed clustering Louvain to check that the results are similar to those obtained from the Leiden clustering. A general purpose of community detection algorithms is identifying communities within a network that are more densely connected internally than with the rest of the network. These algorithms aim to maximize modularity M:

$$M \equiv \frac{1}{2L}\sum_c \left(l_c - \alpha \frac{D_c^2}{2L}\right) \tag{4}$$

where L is the total number of links in the network, l_c is the number of links in community c, α is a resolution parameter, and D_c is the sum of the degrees of the nodes in community c.

The Leiden algorithm begins by assigning each node to its own community and iteratively refines the community structure to improve modularity. After the initial partitioning, the algorithm ensures that nodes within each community are well-connected. It then aggregates the network into a higher-level graph, in which each community is represented as a single node. This process of refinement and aggregation is repeated until no further improvement in community quality can be achieved. Leiden clustering was performed using clusterMaker2 [39] application embedded in Cytoscape with the following options: resolution = 0.5, beta value = 0.01, number of iterations = 2. The chosen resolution parameter influences the size and number of detected communities. We

used 0.5 as a standard setting that balances granularity and interpretability. The beta value adjusts the algorithm's sensitivity to network density, and the specified number of iterations limits the algorithm's refinement process, ensuring computational efficiency while seeking optimal community detection.

Hypergeometric test

After clustering the nodes in the interaction network into several communities (see Results), we investigated whether a certain phylum is enriched in a given cluster. Let us denote the total number of nodes as N and the number of nodes belonging to a given phylum, say phylum A, as M, and also denote the number of nodes in a cluster, say cluster i, as n. If we randomly select n nodes from N nodes, the number of nodes that belong to the phylum A, denoted as K, is a random variable. The probability distribution $P_K(k)$ for for K is given by the hypergeometric distribution:

$$P_K(k) = Pr(K = k) = \frac{\binom{M}{k}\binom{N-M}{n-k}}{\binom{N}{n}} \tag{5}$$

For the observed number $\widehat{k}$ of nodes belonging to the phylum A in the cluster i, we also compute the P-value

$$P_{value \equiv Pr(K \geq k)} \tag{6}$$

If the P-value is less than 0.05, we conclude there are significantly large number of nodes belonging to the phylum A than expected, and hence phylum A is enriched in the cluster i.

Random rewiring of regulatory network

To measure the statistical significancy of the strength of regulations between phyla, we randomized the networks while preserving the in- and out-degree of each node. Self-loops were excluded, and multiple edges were avoided by ensuring that new connections only formed between previously unconnected nodes. For this, we used "rewire" function implemented in a R package "igraph" [40]. We generated empirical distributions of the number of links between phyla by randomly rewired regulatory networks 1,000 times. For the observed number $\widehat{l}$ of links from phylum A to B, we calculate the z-score

$$Z_{score} \equiv \frac{N_l - \langle N_l^{random} \rangle}{\sigma_l^{random}} \tag{7}$$

where N_l is the number of links from phylum A to B, and $\langle N_l^{random} \rangle$ and σ_l^{random} are the mean and standard deviation of links in the randomly rewired networks.

Centrality measures

The out-degree and in-degree of a node i is defined as the number of out-going edges and the number of in-coming edges of the node i, respectively.

The betweenness centrality of a node i is defined as

$$C_i^B \equiv \sum_{j<k}^{N} \frac{d_{jk}(i)}{d_{jk}} \tag{8}$$

where N, d_{jk} and $d_{jk}(i)$ denote the number of nodes, the number of shortest paths between node j and k and the number of shortest paths between node j and k which include node i in the path, respectively.

The closeness centrality of a node i is defined as

$$C_i^B \equiv \sum_{j<k}^{N} \frac{d_{jk(i)}}{d_{jk}} \tag{9}$$

where N and d_{ij} denote the number of nodes and distance between node i and j, respectively.

Network motifs

Network motifs are defined as patterns of interconnections observed more frequently than in an ensemble of randomized networks [41]. We searched for patterns involving two-node and three-node motifs using NetMatch [42] a Cytoscape plugin application.

The statistical significance of each motif was determined through z-scores, calculated by comparing the observed frequency against a null model. This model was generated by randomly shuffling the network's edges 10,000 times, ensuring the degree distribution was maintained. To compare the z-scores of each motif between subject A and subject B, we calculated the z-scores 100 times. This number reflects the maximum number of repetitions supported by NetMatch, which also offered a practical balance between capturing stochastic variability and maintaining computational efficiency.

Results

Microbiota regulatory networks constructed by TENET display power-law degree distribution

With the time-course data on gut microbiota abundance, we calculated TE values for every pair of genera (Supplementary Tables S3-S4). Based on the TE matrix, we constructed gut microbiota regulatory networks for two subjects using TENET with $\theta = 0.01$ (Supplementary Tables S5-S6). After trimming indirect edges, we

measured the network density $\rho \equiv N_e/N_n(N_n-1)$, where N_e and N_n are the number of directed edges and the nodes, respectively. Since the network density ρ is the ratio of the actual number of directed edges to the maximum number of possible directed edges, $0 \leq \rho \leq 1$ We found $\rho = 0.012$ for subject A and $\rho = 0.021$ for subject B, indicating sparsely connected structures. The degree distribution of both networks followed a power-law with degree exponents of $\gamma = 0.913$ for subject A and $\gamma = 1.115$ for subject B (Fig. 1A and B), representing the existence of a few superhub nodes connected with almost every other node, and a large number of nodes with a small number of edges. This sparsity and power-law degree distribution property persisted in the networks constructed with $\theta = 0.05$ (Supplementary Table S7-S8 and Fig. 1C and D). The goodness of fit of the power-law distribution was confirmed by comparing with exponential and log-normal positive distributions, as well as by evaluating the Kolmogorov–Smirnov (KS) statistics, which supported the plausibility of power-law behavior across the networks (Supplementary Table S9).

We then applied Leiden clustering algorithm to discern if these networks exhibit a modular organization [38]. The visualization of the clustering outcomes for subjects A and B is provided in Fig. 2A and B, respectively. The modularity scores M were 0.288 for subject A and 0.35 for subject B, indicating intermediate modularity for both networks (Supplementary Table S10) [43]. This modularity was also found in the constructed network with θ = 0.05 (M = 0.317 for subject A and M = 0.276 for subject B).

Leiden clustering produced four and three clusters for the subject A and B, respectively. These are differentiated by the border colors of the nodes in Fig. 2A and B. To associate each cluster with specific microbial phyla, we color-coded the interior of each node according to the phylum of the represented genus. We enumerated genera within each phylum for every cluster, with the compositional outcomes depicted in Fig. 2C and D for subjects A and B, correspondingly. The color schemes for these figures are consistent with those in Fig. 2A and B. Across all clusters for both subjects, two phyla - *Bacillota* and *Pseudomonadota* - were consistently present. Nevertheless,

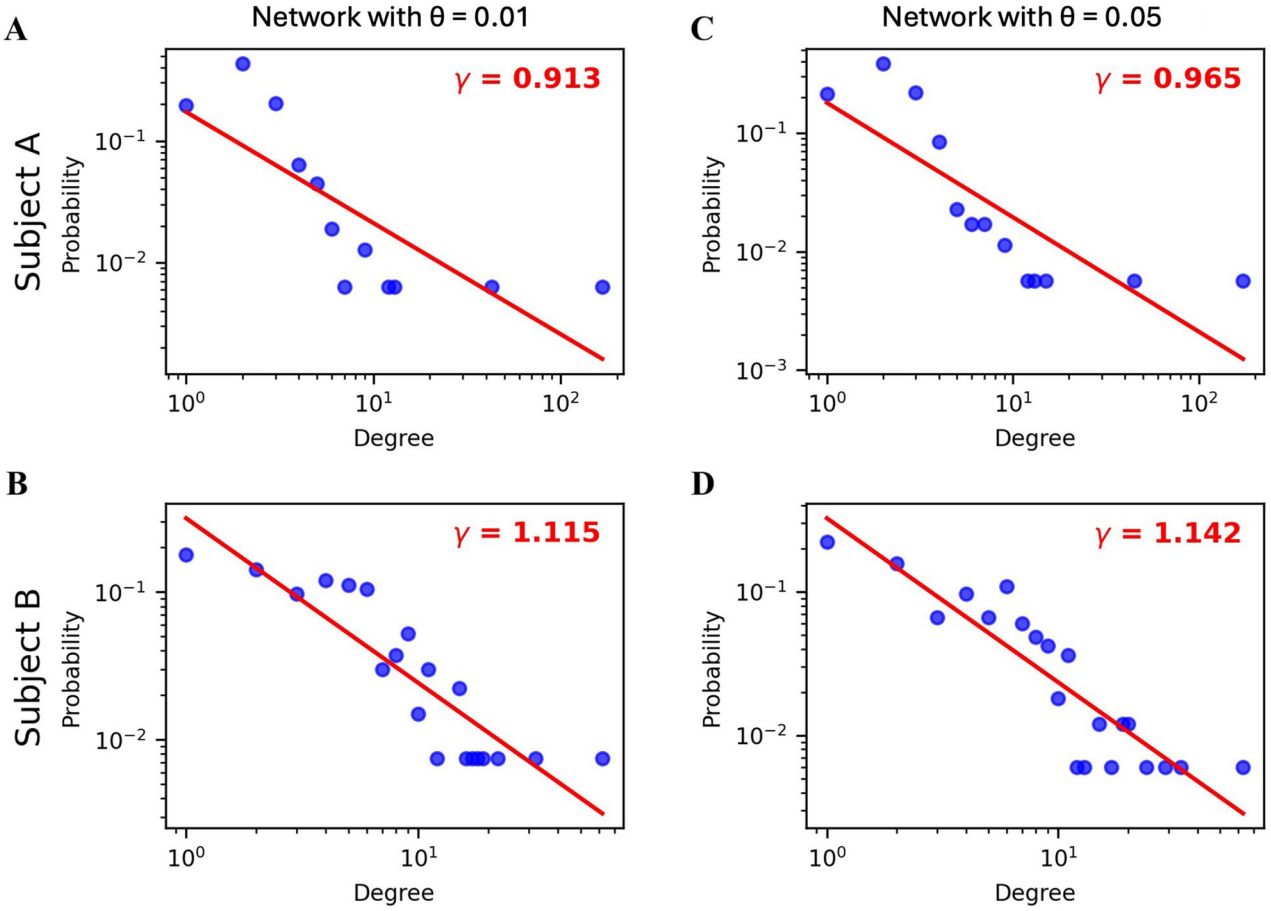

Fig. 1 Gut microbiota regulatory networks display power-law degree distribution. (**A**-**B**) Degree distribution of gut microbiota regulatory networks for subject A (**A**) and B (**B**) with θ = 0.01. (**C**-**D**) Degree distribution of gut microbiota regulatory networks for subject A (**C**) and B (**D**) with θ = 0.05

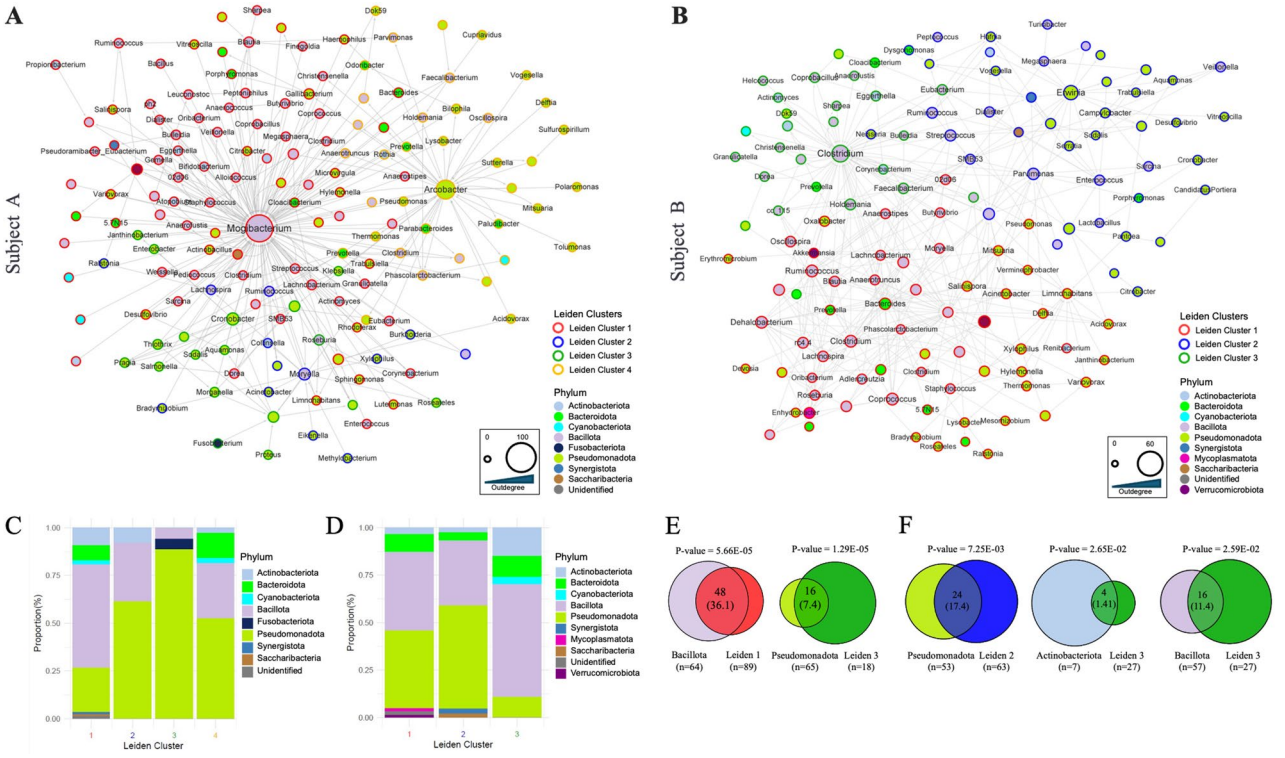

Fig. 2 Gut microbiota regulatory networks exhibit modular structure. (**A-B**) Network representation of gut microbiota regulatory networks for subject A (**A**) and B (**B**) with "Edge-weighted Force directed" layout. The node fill color and border color represent phylum and Leiden cluster, respectively. The node size represents the out-degree. (**C-D**) The fractions of nodes belonging to distinct phyla for each Leiden cluster for subject A (**C**) and B (**D**). (**E-F**) The results of the hypergeometric tests for the phylum compositions for several Leiden clusters in subject A (**E**) and B (**F**). The numbers in the intersection region denote the observed (upper) and expected (lower, presented in parenthesis) number of nodes

the exact phylum compositions differed by cluster. Hypergeometric testing, results of which are shown in Fig. 2E and F, and Supplementary Table S11, identified phyla significantly overrepresented in certain clusters. For instance, *Bacillota* were notably prevalent in Leiden cluster 1 of subject A ($p = 5.66E-5$) and Leiden cluster 3 of subject B ($p = 2.59E-2$), *Pseudomonadota* were enriched in Leiden cluster 3 of subject A ($p = 1.29E-5$) and Leiden cluster 1 of subject B ($p = 7.25E-3$), and *Actinobacteriota* were enriched in Leiden cluster 3 of subject B ($p = 2.65E-2$). Additionally, some phyla appeared exclusively within specific clusters. For example, *Fusobacteriota* were only found in Leiden cluster 3 of Subject A, *Synergistota* were only found in Leiden cluster 1 of subject A and Leiden cluster 2 of subject B, and *Saccharibacteria* were only found in Leiden cluster 1 of subject A and Leiden cluster 2 of subject B. Overall, these findings from our constructed networks reveal discernible communities characterized by unique phyla. The results from the Louvain clustering were similar (Supplementary Table S12).

Random rewiring of the network revealed significant regulatory strengths between phyla

To assess the strength of regulation between phyla, we changed the layout of the networks using Cytoscape by grouping genera with same phylum (Fig. 3A and B). Random rewiring of the networks was performed 1,000 times while preserving the degree distribution, providing z-values of the regulations between phyla (Fig. 3C and D). In both subjects, regulations within *Bacillota* and *Pseudomonadota* were significantly enriched, while regulations between these two phyla were significantly depleted. Interestingly, the regulations from *Fusobacteriota* to *Pseudomonadota* were enriched in the network of subject A (Fig. 3C), whereas the regulations within *Actinobacteriota* and the regulations from *Mycoplasmatota* to *Bacteriodetes* were enriched in the network of subject B (Fig. 3D). These results were consistently found in the constructed network with $\theta = 0.05$ (Supplementary Fig. 1). This suggests that *Fusobacteriota*, *Actinobacteriota*, and *Mycoplasmatota* may play a differential role in the regulation of gut microbiota between the two subjects.

TENET identified key regulatory genera associated with personal experiences

In many network biology studies, there is a common hypothesis that certain key players, or 'hub nodes' play a critical role in maintaining the connections and flow within these networks [44–46]. In some studies, other

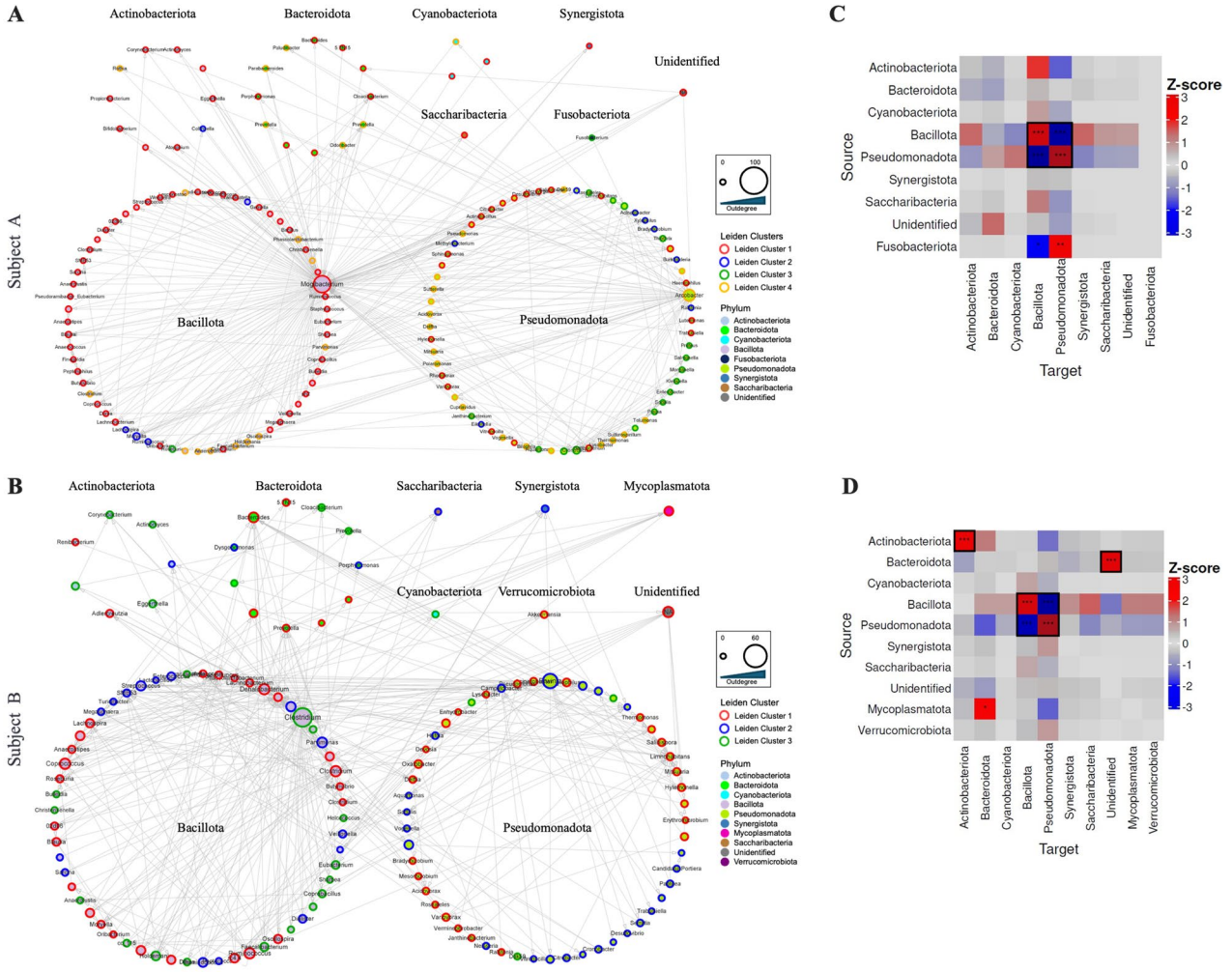

Fig. 3 Random rewiring analysis of gut microbiota regulatory networks reveals significant regulatory relationships between phyla. **A**-**B** Network representation of gut microbiota regulatory networks for subject A (**A**) and B (**B**) with layout of grouping by phyla. The node fill color and border color represent phylum and Leiden cluster, respectively. The node size represents the out-degree. **C**-**D** Heatmaps of the z-scores of the number of regulations between phyla for subject A (**C**) and B (**D**). The networks were obtained with θ = 0.01. Statistical significance is indicated by asterisks for unadjusted p-values ($P < 0.05$ (*), $P < 0.01$ (**), and $P < 0.001$ (***)) and by black boxes indicating FDR < 0.05

measures of the importance of these hubs, such as their role as connectors or how centrally located they are in the network (i.e. betweenness or closeness), might be better at pinpointing critical proteins or genes [47–49]. To investigate this idea in the microbiota regulatory networks, we calculated four centrality measures: out-degree, in-degree, betweenness, and closeness (Fig. 4). The centrality analysis revealed subject-specific key regulatory genera. In subject A, the genera *Mogibacterium*, belonging to the family *Mogibacteriaceae*, and *Arcobacter*, belonging to the family *Campylobacteraceae*, were consistently identified as key players across all four measurement methods (Fig. 4A). However, in subject B, the genus *Clostridium*, belonging to the family *Ruminococcaceae*, ranked first by out-degree, in-degree, and betweenness centrality, but not by closeness centrality (Fig. 4B). Instead, two different genera *Dysgonomonas*, belonging to the family *Porphyromonadaceae*, and *Peptococcus*, belonging to the family *Peptococcaceae*, were top ranked in closeness. This indicates that *Dysgonomonas* and *Peptococcus* play a bridge role between modules instead of being a local hub. These key regulatory genera were also found in the regulatory networks constructed with θ = 0.05 (Supplementary Fig. 2).

As a comparative analysis, we additionally constructed microbial association networks using eLSA, a time-series-aware algorithm [16]. Specifically, we applied eLSA to each subject's time-series data using robust Z normalization and 100 permutations optimized for delayed interaction detection, with edges filtered at q < 0.01 and indirect edges removed using the same trimming strategy as in TENET. *Arcobacter*, identified as a hub genus by TENET, also ranked highest in in-degree centrality within the eLSA-derived network. However,

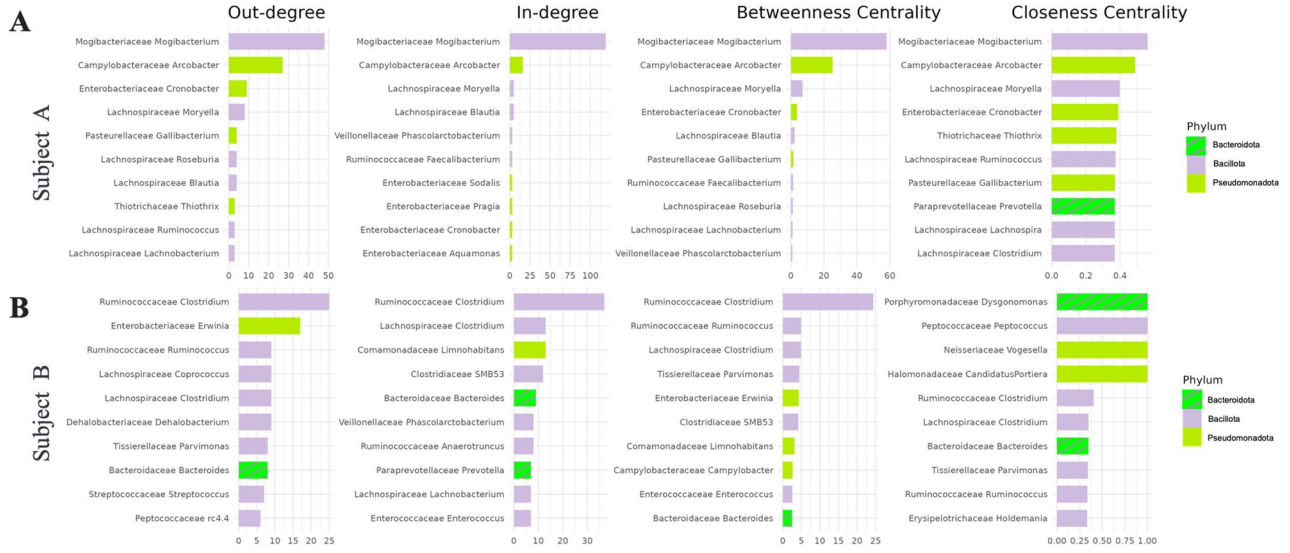

Fig. 4 Centrality analysis of gut microbiota regulatory networks reveals candidates of key regulatory genera for regulating gut microbiota. **A**-**B** Four centrality measures (outdegree, indegree, betweenness centrality, and closeness centrality) of subject A (**A**) and B (**B**). The color for bar represents phylum. The networks were obtained with $\theta = 0.01$

Mogibacterium, another top TENET-inferred hub, did not appear in the top 10 based on any centrality measure in eLSA. Instead, a broader set of microbial genera emerged as central nodes, reflecting method-specific sensitivity in identifying regulatory hubs. TENET facilitated the discovery of interpretable hubs, such as Clostridium in Subject B, highlighting plausible microbial drivers that may play a role in post-infection dynamics (Supplementary Fig. 3). To test the significance of these results, we applied a fully randomized procedure—jointly shuffling temporal order and taxon identities—and reconstructed networks with TENET. We compared shuffled and original networks in terms of node/edge overlap and hub metrics; in both subjects, the overall structure of the original TENET-inferred networks was not preserved under this randomization (Supplementary Fig. 4).

To further benchmark network inference approaches, we explored two additional network inference algorithm, correlation network and SpiecEasi [36]. We calculated the degree of the resulting networks, as both algorithms yield undirected graphs. For Subject A, the top 10 genera by degree did not include pathogens highlighted in the original study. In contrast, in the correlation network of Subject B, the genus *Edwardsiella*, particularly *Edwardsiella tarda*, was identified due to its known association with food- and waterborne infection [50] (Supplementary Fig. 5).

To evaluate the impact of data compositionality, we transformed genus-level abundances using both centered log-ratio (CLR) and log-normalization. We then reconstructed the TENET networks and calculated four centrality measures (outdegree, indegree, betweenness centrality, and closeness centrality) for both Subject A and Subject B (Supplementary Fig. 6). Interestingly, after normalization, the key taxa previously identified as network hubs—including those highly relevant to the study's clinical context—no longer ranked among the top 10 central genera. This finding suggests that these standard transformations, while statistically valid, may mask the specific biological signals that TENET is designed to identify from abundance data.

We further assessed robustness by removing time points associated with major perturbation events. For Subject A, exclusion of the travel period had minimal impact, with *Mogibacterium* and *Arcobacter* still ranking highly by outdegree. Similarly, in Subject B, removal of the food poisoning interval did not alter the centrality of *Clostridium*, which remained the top-ranked genus by outdegree, while *Dysgonomonas* and *Peptococcus* continued to fall outside the top 10 (Supplementary Fig. 7). To examine whether this robustness holds under more generalized data loss, we next evaluated centrality stability following random removal of 10%, 20%, and 30% of time points, preserving temporal order. In Subject A, *Mogibacterium* and *Arcobacter* remained highly ranked by outdegree up to 30% removal. In Subject B, Clostridium was stable with 30% removed (Supplementary Figs. 8–9).

In addition, we tested the impact of a longer time lag by setting the lag parameter to $L = 2$ instead of $L = 1$. For Subject A, while the set of nodes remained unchanged, modest structural differences were observed in the resulting network. Specifically, 11 edges present in the $L = 1$ network disappeared in the $L = 2$ network, one edge (from *Mogibacterium* to *Desulfovibrio*) reversed its direction, and 14 new edges emerged. Among the lost connections, two outgoing edges from *Mogibacterium* and

one from *Arcobacter* were removed. In contrast, for Subject B, no changes were observed in either the node set or edge structure between the L = 1 and L = 2 networks (Supplementary Fig. 10).

For the centrality analysis results, Subject A experienced traveler's diarrhea (TD) while traveling to Southeast Asia. *Acrobacter*, one of the key regulatory genera, displayed peak abundance right after the traveling period (Fig. 5A) [51–57].

Subject B experienced food poisoning, which was consistent with an increase in sequencing reads of *Enterobacteriaceae Salmonella* during the infection period. However, the network for Subject B indicates that *Clostridium*, part of the *Bacillota* phylum, displayed the highest out-degree and in-degree, the second highest betweenness centrality, and the fifth highest closeness centrality. Notably, *Salmonella* did not appear in the list of top 10 key genera based on these centralities. We corroborated a significant increase in the abundance of *Clostridium* after infection (Fig. 5B) [31]. Phyla that were significantly enriched in specific Leiden clusters showed consistent temporal abundance patterns across the time series (Supplementary Fig. 11).

Differential enrichment of feedback loops in two subject's networks

In the original longitudinal microbiome study, the authors proposed that the microbiota of the two subjects demonstrated different recovery dynamics [31]. The microbiota community from subject A showed reversible

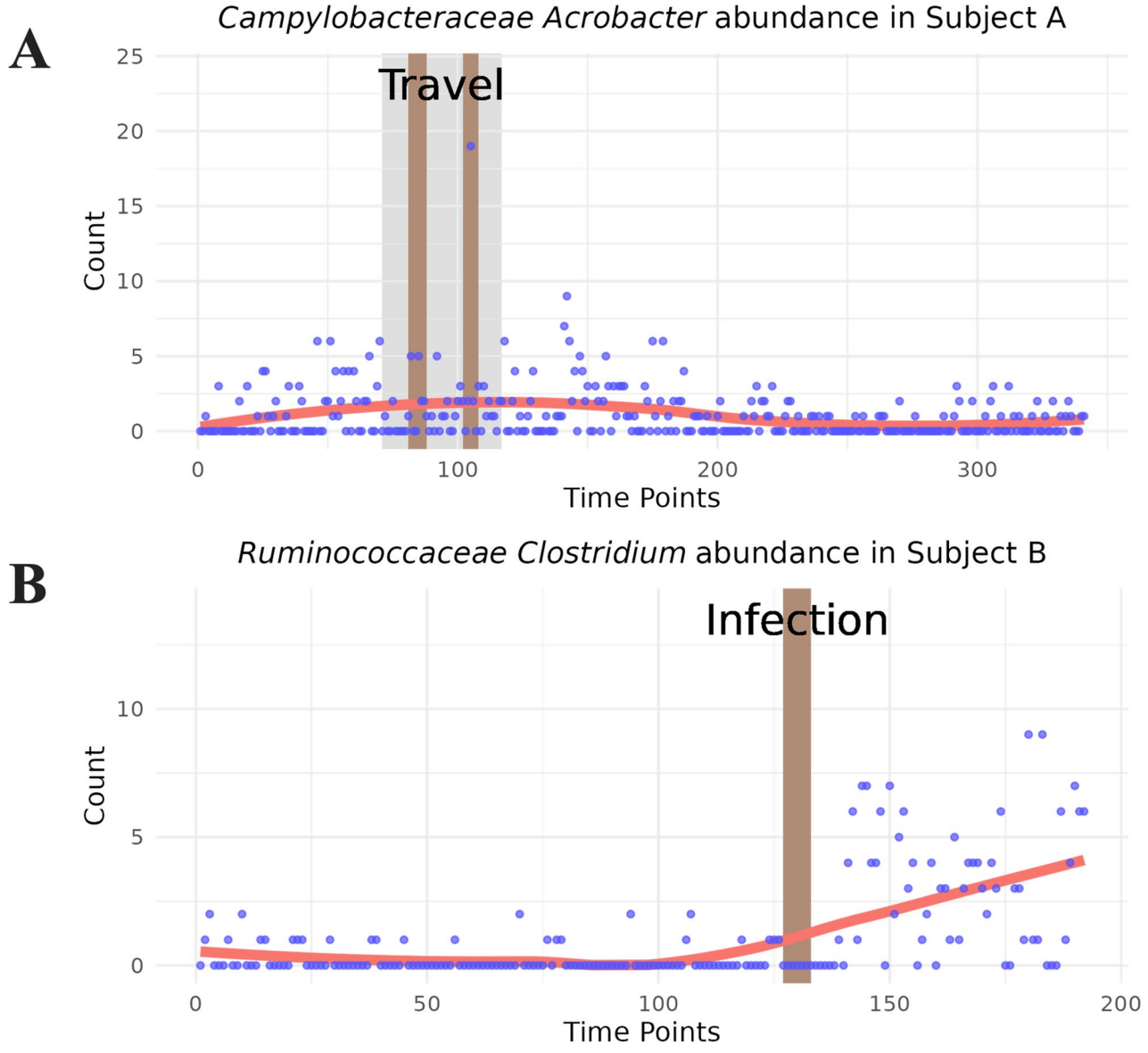

Fig. 5 Time-course abundance of key regulatory microbiota. **A**-**B** Time course abundance of *Acrobacter* in subject A (**A**) and *Clostridium* in subject B (**B**)

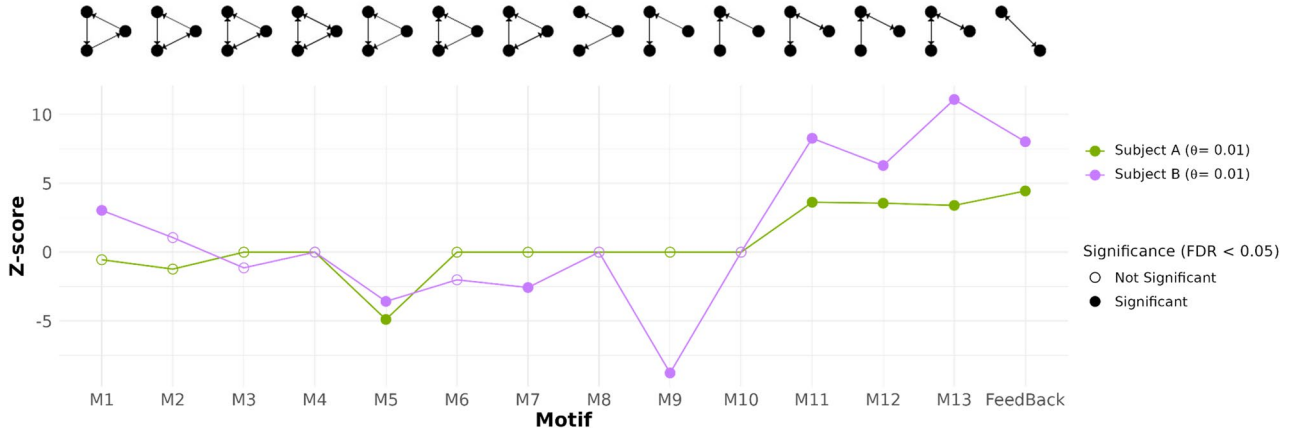

Fig. 6 The enrichment of feedback loops in gut microbiota regulatory network. The significance of network motifs of two-node and three-node were obtained by random shuffling 10,000 times from the networks for subject A and subject B with θ = 0.01. Motif significance was assessed via z-scores, with FDR correction applied

dynamics after traveling abroad, whereas that from subject B showed irreversible changes after an enteric infection. To further investigate the differential recovery dynamics, we searched for network motifs, including a two-node feedback loop and thirteen possible three-node motifs, based on the relevance between feedback loops and steady-state dynamics [58, 59]. The results showed differential enrichment of feedback loops between the two subjects (Fig. 6). Both the two-node feed-back loop and three three-node motifs associated with the two-node feedback loops (M11, M12, and M13) were significantly enriched in both networks. However, the significance levels of these four motifs were much higher in subject B's network (z-score and p-value = 8.03 and 4.44E-16 for two-node feedback loop, 8.28 and 1.11E-16 for M11, 6.3 and 1.49E-10 for M12, and 11.1 and 6.27E-29 for M13) than in subject A's network (z-score and p-value = 4.45 and 4.29E-6 for two-node feedback loop, 3.63 and 1.42E-4 for M11, 3.56 and 1.85E-4 for M12, and 3.4 and 3.37E-4 for M13). On the other hand, motif M9 representing cascade was only observed in Subject B's network, with a z-score of −8.43 and a p-value of 1.48E-16. Consistent results were also obtained from the constructed networks with θ = 0.05 (Supplementary Fig. 12). These differential enrichment and depletion of motifs between two subjects' networks, was consistent when we repeated motif analysis 100 times (Supplementary Fig. 13). This finding suggests that feedback loops may be a critical factor in the differential recovery dynamics.

Discussion

In this paper, we employed TENET to construct regulatory networks using longitudinal gut microbiota data from two subjects. TENET, known for its efficacy in identifying key regulatory factors in gene expression regulation from pseudotime-ordered single cell RNAseq data [26], was adapted for the analysis of time-course microbiota data. TENET was originally designed for constructing gene regulatory networks in single-cell data, its application was justified here because microbiota abundance data basically share the same data type format; read count. A challenge of this application lies in the difficulty of obtaining publicly accessible, high-quality data suitable for the application of transfer entropy. Despite of this challenge, this approach not only enabled us to measure the regulatory strength between phyla but also facilitated the identification of key regulatory genera, such as *Arcobacter* and *Mogibacterium* in subject A, and *Clostridium*, *Dysgonomonas*, and *Peptococcus* in subject B. Notably, the top key regulatory genera were found to be associated with distinct experiences of each subject. For example, subject A exhibited *Acrobacter* as a key genus, linked to his or her experience of traveler's diarrhea. *Acrobacter* is a microbial genus belonging to the *Pseudomonadota* phylum and is associated with TD, which is frequently encountered in Southeast Asia [51–53]. Specifically, *A. butzleri*, one of the *Acrobacter* species has been extensively studied and demonstrated to have considerable importance for TD [54–57]. Meanwhile, subject B experienced food poisoning with an increase in sequencing reads of *Enterobacteriaceae Salmonella*. Although *Salmonella* did not appear as a key genus, our network analysis identified *Clostridium* (part of the *Bacillota* phylum) as a key regulatory genus. This is consistent with findings from the original study, which noted a significant increase in a *Bacillota*-dominated OTU cluster, including *Clostridium*, following the infection. The sustained elevated abundance of this cluster implies a loss of compositional stability in subject B's microbiota, suggesting that *Clostridium* may play a regulatory role in counteracting the external infection [31].

Many studies have been discovered that *Bacillota*, a category of intestinal microorganisms, have a substantial impact on modulating the body's immune system [60]. During digestion, *Bacillota* release glycoconjugates, which stimulate the production of the cytokine IL-34, leading to an enhancement of the immune response. Despite their presence throughout the body, immune balance is maintained through a feedback control mechanism. Smaller glycoconjugates are effectively managed by albumin, preventing excessive immune responses. Our study, through its observations of microbial community structures, suggests that certain *Bacillota* genera may play a role in hist systemic immunity. *Clostridium*, predominantly classified within the *Bacillota* phylum, encompasses a variety of strains that are commonly found in diverse environments, including soil, sewage, the digestive tracts, and water. While some species within the *Clostridium* genus serve useful functions, others have the potential to produce toxins or cause infections, posing potential risks to the health of both humans and animals [61, 62]. The original study of this time-course microbiota data suggested that Subject A's gut microbiota reverted to its pre-travel state, whereas Subject B's gut microbiota did not return to its pre-infection state and switched to a new stable state. The centrality of *Clostridium* in Subject B's microbial network suggests its potential role in establishing a new steady state following *Salmonella* infection. Certain *Clostridium* species, such as *Clostridium butyricum*, have been shown to modulate host immunity by inducing IL-10-producing macrophages, thereby contributing to intestinal homeostasis [63]. Moreover, insights from network-based modeling indicate that central taxa like *Clostridium* can play pivotal roles in regulating community dynamics and facilitating transitions to alternative stable states in response to ecological perturbations [64].

To compare the structural difference between two subjects' networks, we investigated three global network measures including degree distribution, modularity, and motif enrichment. We found that the degree exponent and modularity were comparable in the two networks. However, the enrichment of the two-node feedback loops and three-node motif coupled with two-node feedback loops were more enriched in the network for subject B than the network for subject (A) On the other hand, cascade motif was depleted only in the network for subject (B) Feedback loops and coupled feedback loops have been suggested to evolve to support multiple steady states or hysteresis [58, 65]. These structures may also be related to resilience or functional redundancy in microbial networks, where feedback interactions are thought to support stability and recovery following disturbance [66, 67]. Consistent with this, the original study reported that Subject A's gut microbiota reverted to its pre-travel state, whereas Subject B's gut microbiota did not return to its pre-infection state but instead transitioned to a new stable state. Thus, subject B's network topology, enriched with feedback motifs and lacking cascade motifs, may reflect a shift toward a new equilibrium, while Subject A's network, may favorable reversible dynamics. These contrasting motif enrichment between two subjects underscores their potential critical impact on varying recovery dynamics.

Motif studies span both biomolecular and ecological networks, including trophic modules in microbial communities [41]. By identifying recurring interaction patterns, motif analysis highlights how species-level interactions underpin community robustness and adaptability to environmental changes [37]. In our study, motifs involving taxa such as *Faecalibacterium*, *Clostridium*, and *Roseburia*—well-known for their roles in short-chain fatty acid metabolism—suggest underlying trophic or syntrophic relationships [68, 69]. Additionally, feedback interactions between *Bacillota* and facultative anaerobic *Pseudomonadota* may reflect syntrophic oxygen-scavenging processes that promote anaerobic stability [70]. These insights suggest that motif-level analyses in longitudinal microbiome studies can inform predictions of community resilience and state transitions.

The random rewiring of the microbiota regulatory networks of gut microbiota highlights the significant directional relationships between phyla. In both subjects, regulations within *Firmicutes* or *Proteobacteria* are markedly enriched, while regulations between these two phyla are significantly reduced. This suggests that microbiota preferentially regulate taxa within the same phylum rather than across different phyla. Such within-phylum regulatory preference may stem from underlying functional coherence and evolutionary relatedness, as closely related microbes are more likely to share compatible signaling systems, metabolic pathways, and ecological roles [71, 72]. This phylo-functional alignment may, in turn, promote more efficient regulatory coordination and help explain the modular network structures observed in our study, where regulatory interactions are largely confined within phylogenetic boundaries [71, 72].

Our findings are based on only two individuals and thus limits the generalizability of the results. Future studies should apply TENET to larger longitudinal cohorts encompassing diverse lifestyles, dietary interventions, and perturbations to verify whether the regulatory principles identified here—subject-specific hub taxa, preferential within-phylum control, and feedback-loop-enriched topology—hold across populations. Integrating additional multi-omics layers, such as metabolomics or host transcriptomics, will help clarify how microbial network dynamics influence host responses.

In conclusion, this study leveraged TENET to construct regulatory networks of longitudinal gut microbiota data. The adapted approach allowed precise measurement of regulatory strength between phyla and identification of key regulatory genera linked to subject-specific experiences. Despite the small sample size, our findings provide insights into the roles of *Bacillota*, especially *Clostridium*, in modulating immunity and demonstrate TENET's promise for analyzing large-scale time-series microbiota datasets. Multiomics data including metabolomics or host transcriptomic data may further elucidate how microbial network dynamics influence host responses.

Supplementary Information

The online version contains supplementary material available at https://doi.org/10.1186/s12864-025-12384-1.

Supplementary Material 1

Supplementary Material 2

Acknowledgements
We are grateful to Professor Daewon Lee and Professor Sunjae Lee for their constructive and enthusiastic comments.

Authors' contributions
J.K. and J.L. planned the experiment, C.P., J.K. and J.L. wrote the manuscript and C.P., J.K. and J.L. analyzed data.

Funding
This work was supported by the National Research Foundation of Korea, funded by the Ministry of Science and ICT (NRF-2020R1A2C1005956) to JL and Basic Science Research Program through the National Research Foundation of Korea (NRF) funded by the Ministry of Education (RS-2023-00220207, RS-2024-00342721, RS-2024-00440285) to JK.

Data availability
The raw 16 S rRNA V4 sequencing data analyzed in this study are publicly available in the European Nucleotide Archive (ENA) under BioProject accession PRJEB6518. Post-processed microbiome time-series profiles generated by the MGnify pipeline (version 2.0) can be accessed at MGYS00001278. These processed datasets include 32 phyla and 879 operational taxonomic units (OTUs), which we further aggregated to 667 genera for down-stream analysis (see Supplementary Tables S1–S2). The TENET algorithm used to infer causal interaction networks was obtained from the official GitHub repository (https://github.com/neocaleb/TENET).

Declarations

Ethics approval and consent to participate
Not applicable.

Consent for publication
Not applicable.

Competing interests
The authors declare no competing interests.

Received: 25 February 2025 / Accepted: 27 November 2025
Published online: 05 December 2025

References

1. Cho I, Yamanishi S, Cox L, Methé BA, Zavadil J, Li K, Gao Z, Mahana D, Raju K, Teitler I. Antibiotics in early life alter the murine colonic Microbiome and adiposity. Nature. 2012;488(7413):621–6.
2. Turnbaugh PJ, Ridaura VK, Faith JJ, Rey FE, Knight R, Gordon JI. The effect of diet on the human gut microbiome: a metagenomic analysis in humanized gnotobiotic mice. Sci Transl Med. 2009;1(6):ra614–1614.
3. Buffie CG, Jarchum I, Equinda M, Lipuma L, Gobourne A, Viale A, Ubeda C, Xavier J, Pamer EG. Profound alterations of intestinal microbiota following a single dose of clindamycin results in sustained susceptibility to clostridium difficile-induced colitis. Infect Immun. 2012;80(1):62–73.
4. Turnbaugh PJ, Ley RE, Mahowald MA, Magrini V, Mardis ER, Gordon JI. An obesity-associated gut Microbiome with increased capacity for energy harvest. Nature. 2006;444(7122):1027–31.
5. Devkota S, Wang Y, Musch MW, Leone V, Fehlner-Peach H, Nadimpalli A, Antonopoulos DA, Jabri B, Chang EB. Dietary-fat-induced taurocholic acid promotes pathobiont expansion and colitis in Il10–/– mice. Nature. 2012;487(7405):104–8.
6. Heiss CN, Olofsson LE. Gut microbiota-dependent modulation of energy metabolism. J Innate Immun. 2018;10(3):163–71.
7. Ye H, Borusak S, Eberl C, Krasenbrink J, Weiss AS, Chen S-C, Hanson BT, Hausmann B, Herbold CW, Pristner M. Ecophysiology and interactions of a taurine-respiring bacterium in the mouse gut. Nat Commun. 2023;14(1):5533.
8. Maciel-Fiuza MF, Muller GC, Campos DMS, do, Socorro Silva Costa P, Peruzzo J, Bonamigo RR, Veit T, Vianna FSL. Role of gut microbiota in infectious and inflammatory diseases. *Frontiers in microbiology* 2023, 14:1098386.
9. Sommer F, Bäckhed F. The gut microbiota—masters of host development and physiology. Nat Rev Microbiol. 2013;11(4):227–38.
10. Johnson AJ, Vangay P, Al-Ghalith GA, Hillmann BM, Ward TL, Shields-Cutler RR, Kim AD, Shmagel AK, Syed AN, Walter J. Daily sampling reveals personalized diet-microbiome associations in humans. Cell Host Microbe. 2019;25(6):789–802. e785.
11. Faust K, Sathirapongsasuti JF, Izard J, Segata N, Gevers D, Raes J, Huttenhower C. Microbial co-occurrence relationships in the human Microbiome. PLoS Comput Biol. 2012;8(7):e1002606.
12. Reshef DN, Reshef YA, Finucane HK, Grossman SR, McVean G, Turnbaugh PJ, Lander ES, Mitzenmacher M, Sabeti PC. Detecting novel associations in large data sets. Science. 2011;334(6062):1518–24.
13. Friedman J, Alm EJ. Inferring correlation networks from genomic survey data. 2012.
14. Segata N, Boernigen D, Tickle TL, Morgan XC, Garrett WS, Huttenhower C. Computational meta'omics for microbial community studies. Mol Syst Biol. 2013;9(1):666.
15. Ruan Q, Dutta D, Schwalbach MS, Steele JA, Fuhrman JA, Sun F. Local similarity analysis reveals unique associations among marine bacterioplankton species and environmental factors. Bioinformatics. 2006;22(20):2532–8.
16. Xia LC, Steele JA, Cram JA, Cardon ZG, Simmons SL, Vallino JJ, Fuhrman JA, Sun F. Extended local similarity analysis (eLSA) of microbial community and other time series data with replicates. In: *BMC systems biology:* Springer; 2011: 1–12.
17. Xia LC, Ai D, Cram J, Fuhrman JA, Sun F. Efficient statistical significance approximation for local similarity analysis of high-throughput time series data. Bioinformatics. 2013;29(2):230–7.
18. Stein RR, Bucci V, Toussaint NC, Buffie CG, Rätsch G, Pamer EG, Sander C, Xavier JB. Ecological modeling from time-series inference: insight into dynamics and stability of intestinal microbiota. PLoS Comput Biol. 2013;9(12):e1003388.
19. Faust K, Bauchinger F, Laroche B, De Buyl S, Lahti L, Washburne AD, Gonze D, Widder S. Signatures of ecological processes in microbial community time series. Microbiome. 2018;6:1–13.
20. Lugo-Martinez J, Ruiz-Perez D, Narasimhan G, Bar-Joseph Z. Dynamic interaction network inference from longitudinal Microbiome data. Microbiome. 2019;7(1):54.
21. Fujita H, Ushio M, Suzuki K, Abe MS, Yamamichi M, Okazaki Y, Canarini A, Hayashi I, Fukushima K, Fukuda S. Facilitative interaction networks in experimental microbial community dynamics. Front Microbiol. 2023;14:1153952.
22. Schreiber T. Measuring information transfer. Phys Rev Lett. 2000;85(2):461.
23. Orlandi JG, Stetter O, Soriano J, Geisel T, Battaglia D. Transfer entropy reconstruction and labeling of neuronal connections from simulated calcium imaging. PLoS ONE. 2014;9(6):e98842.

24. Wollstadt P, Martínez-Zarzuela M, Vicente R, Díaz-Pernas FJ, Wibral M. Efficient transfer entropy analysis of non-stationary neural time series. PLoS ONE. 2014;9(7):e102833.
25. Spinney RE, Prokopenko M, Lizier JT. Transfer entropy in continuous time, with applications to jump and neural spiking processes. Phys Rev E. 2017;95(3):032319.
26. Kim J, Jakobsen T, Natarajan S, Won KN. TENET: gene network reconstruction using transfer entropy reveals key regulatory factors from single cell transcriptomic data. Nucleic Acids Res. 2021;49(1):e1–1.
27. Kim D, Kim J, Yu YS, Kim YR, Baek SH, Won K-J. Systemic approaches using single cell transcriptome reveal that C/EBPγ regulates autophagy under amino acid starved condition. Nucleic Acids Res. 2022;50(13):7298–309.
28. Weng G, Kim J, Won KJ. VeTra: a tool for trajectory inference based on RNA velocity. Bioinformatics. 2021;37(20):3509–13.
29. Kwon O, Yang J-S. Information flow between stock indices. Europhys Lett. 2008;82(6):68003.
30. Kim M, Newth D, Christen P. Macro-level information transfer in social media: reflections of crowd phenomena. Neurocomputing. 2016;172:84–99.
31. David LA, Materna AC, Friedman J, Campos-Baptista MI, Blackburn MC, Perrotta A, Erdman SE, Alm EJ. Host lifestyle affects human microbiota on daily timescales. Genome Biol. 2014;15:1–15.
32. Armour CR, Topçuoğlu BD, Garretto A, Schloss PD. A goldilocks principle for the gut microbiome: taxonomic resolution matters for microbiome-based classification of colorectal cancer. MBio. 2022;13(1):e03161–03121.
33. Oren A, Garrity GM. Valid publication of the names of forty-two phyla of prokaryotes. Int J Syst Evol MicroBiol. 2021;71(10):005056.
34. Benjamini Y, Hochberg Y. Controlling the false discovery rate: a practical and powerful approach to multiple testing. J Roy Stat Soc: Ser B (Methodol). 1995;57(1):289–300.
35. Shannon P, Markiel A, Ozier O, Baliga NS, Wang JT, Ramage D, Amin N, Schwikowski B, Ideker T. Cytoscape: a software environment for integrated models of biomolecular interaction networks. Genome Res. 2003;13(11):2498–504.
36. Kurtz ZD, Müller CL, Miraldi ER, Littman DR, Blaser MJ, Bonneau RA. Sparse and compositionally robust inference of microbial ecological networks. PLoS Comput Biol. 2015;11(5):e1004226.
37. Bascompte J, Stouffer DB. The assembly and disassembly of ecological networks. Philos Trans R Soc Lond B Biol Sci. 2009;364(1524):1781–7.
38. Traag VA, Waltman L, Van Eck NJ. From Louvain to leiden: guaranteeing well-connected communities. Sci Rep. 2019;9(1):1–12.
39. Morris JH, Apeltsin L, Newman AM, Baumbach J, Wittkop T, Su G, Bader GD. Ferrin TE: clustermaker: a multi-algorithm clustering plugin for cytoscape. BMC Bioinformatics. 2011;12:1–14.
40. Csardi G, Nepusz T. The Igraph software. Complex Syst. 2006;1695:1–9.
41. Milo R, Shen-Orr S, Itzkovitz S, Kashtan N, Chklovskii D, Alon U. Network motifs: simple Building blocks of complex networks. Science. 2002;298(5594):824–7.
42. Ferro A, Giugno R, Pigola G, Pulvirenti A, Skripin D, Bader GD, Shasha D. NetMatch: a cytoscape plugin for searching biological networks. Bioinformatics. 2007;23(7):910–2.
43. Newman ME. Modularity and community structure in networks. *Proceedings of the national academy of sciences* 2006, 103(23):8577–8582.
44. Barabasi A-L, Oltvai ZN. Network biology: Understanding the cell's functional organization. Nat Rev Genet. 2004;5(2):101–13.
45. Jeong H, Mason SP, Barabási A-L, Oltvai ZN. Lethality and centrality in protein networks. Nature. 2001;411(6833):41–2.
46. Han J-DJ, Bertin N, Hao T, Goldberg DS, Berriz GF, Zhang LV, Dupuy D, Walhout AJ, Cusick ME, Roth FP. Evidence for dynamically organized modularity in the yeast protein–protein interaction network. Nature. 2004;430(6995):88–93.
47. Ashtiani M, Salehzadeh-Yazdi A, Razaghi-Moghadam Z, Hennig H, Wolkenhauer O, Mirzaie M, Jafari M. A systematic survey of centrality measures for protein-protein interaction networks. BMC Syst Biol. 2018;12:1–17.
48. Koschützki D, Schreiber F. Centrality analysis methods for biological networks and their application to gene regulatory networks. Gene Regul Syst Biology. 2008;2:GRSB. S702.
49. Li M, Zhang H, Wang J-x, Pan Y. A new essential protein discovery method based on the integration of protein-protein interaction and gene expression data. BMC Syst Biol. 2012;6:1–9.
50. Hasegawa K, Kenya M, Suzuki K, Ogawa Y. Characteristics and prognosis of patients with Edwardsiella Tarda bacteremia at a single institution, Japan, 2005–2022. Ann Clin Microbiol Antimicrob. 2022;21(1):56.
51. Jiang Z, DuPont H. Etiology of travellers' diarrhea. J Travel Med. 2017;24(suppl1):S13–6.
52. López-Vélez R, Lebens M, Bundy L, Barriga J, Steffen R. Bacterial travellers' diarrhoea: A narrative review of literature published over the past 10 years. Travel Med Infect Dis. 2022;47:102293.
53. Teague NS, Srijan A, Wongstitwilairoong B, Poramathikul K, Champathai T, Ruksasiri S, Pavlin J, Mason CJ. Enteric pathogen sampling of tourist restaurants in Bangkok, Thailand. J Travel Med. 2010;17(2):118–23.
54. Vandenberg O, Dediste A, Houf K, Ibekwem S, Souayah H, Cadranel S, Douat N, Zissis G, Butzler JP, Vandamme P. Arcobacter species in humans. Emerg Infect Dis. 2004;10(10):1863–7.
55. Collado L, Figueras MJ. Taxonomy, epidemiology, and clinical relevance of the genus Arcobacter. Clin Microbiol Rev. 2011;24(1):174–92.
56. Chieffi D, Fanelli F, Fusco V. Arcobacter butzleri: Up-to-date taxonomy, ecology, and pathogenicity of an emerging pathogen. Compr Rev Food Sci Food Saf. 2020;19(4):2071–109.
57. Prouzet-Mauléon V, Labadi L, Bouges N, Ménard A, Mégraud F. Arcobacter butzleri: underestimated enteropathogen. Emerg Infect Dis. 2006;12(2):307–9.
58. Kim J, Kim TG, Jung SH, Kim JR, Park T, Heslop-Harrison P, Cho KH. Evolutionary design principles of modules that control cellular differentiation: consequences for hysteresis and multistationarity. Bioinformatics. 2008;24(13):1516–22.
59. Prill RJ, Iglesias PA, Levchenko A. Dynamic properties of network motifs contribute to biological network organization. PLoS Biol. 2005;3(11):e343.
60. Jordan CKI, Brown RL, Larkinson MLY, Sequeira RP, Edwards AM, Clarke TB. Symbiotic firmicutes Establish mutualism with the host via innate tolerance and resistance to control systemic immunity. Cell Host Microbe. 2023;31(9):1433–e14491439.
61. Poutanen SM, Simor AE. Clostridium difficile-associated diarrhea in adults. CMAJ. 2004;171(1):51–8.
62. Ducarmon QR, Zwittink RD, Hornung BVH, van Schaik W, Young VB, Kuijper EJ. Gut microbiota and colonization resistance against bacterial enteric infection. Microbiol Mol Biol Rev. 2019;83(3):e00007-19.
63. Kanai T, Mikami Y, Hayashi A. A breakthrough in probiotics: clostridium Butyricum regulates gut homeostasis and anti-inflammatory response in inflammatory bowel disease. J Gastroenterol. 2015;50:928–39.
64. Goyal A, Dubinkina V, Maslov S. Multiple stable States in microbial communities explained by the stable marriage problem. ISME J. 2018;12(12):2823–34.
65. Kim JR, Yoon Y, Cho KH. Coupled feedback loops form dynamic motifs of cellular networks. Biophys J. 2008;94(2):359–65.
66. Coyte KZ, Schluter J, Foster KR. The ecology of the microbiome: networks, competition, and stability. Science. 2015;350(6261):663–6.
67. Allison SD. JB <>Martiny 2008 Resistance, resilience, and redundancy in microbial communities. Proc Natl Acad Sci 105 supplement_1 11512–9.
68. Louis P, Flint HJ. Formation of propionate and butyrate by the human colonic microbiota. Environ Microbiol. 2017;19(1):29–41.
69. Flint HJ, Scott KP, Duncan SH, Louis P, Forano E. Microbial degradation of complex carbohydrates in the gut. Gut Microbes. 2012;3(4):289–306.
70. Wang SP, Rubio LA, Duncan SH, Donachie GE, Holtrop G, Lo G, Farquharson FM, Wagner J, Parkhill J, Louis P. Pivotal roles for pH, lactate, and lactate-utilizing bacteria in the stability of a human colonic microbial ecosystem. Msystems. 2020;5(5). https://doi.org/10.1128/msystems. 00645 – 00620.
71. Aguirre de Cárcer D. A conceptual framework for the phylogenetically constrained assembly of microbial communities. Microbiome. 2019;7(1):142.
72. Parras-Moltó M, Aguirre de Carcer D: Assessment of phylo-functional coherence along the bacterial phylogeny and taxonomy. Scientific Reports 2021, 11(1):8299.

Publisher's Note